Rare Metal Materials and Engineering
Volume 50, Issue 7, July 2021
Available online at www.rmme.ac.cn

Science Press

Cite this article as: Liu Guanglei, Cao Yuhao, Ji Sibo, et al. Effect of Laser Clad Ni60A Coating on High Temperature Dry Sliding Friction and Wear Characteristics of 20CrNiMo Steel[J]. Rare Metal Materials and Engineering, 2021, 50(07): 2281-2287.

ARTICLE

Effect of Laser Clad Ni60A Coating on High Temperature Dry Sliding Friction and Wear Characteristics of 20CrNiMo Steel

Liu Guanglei, Cao Yuhao, Ji Sibo, Yu Hui, Jiang Wenneng, Li Maojun, Si Naichao

School of Materials Science and Engineering, Jiangsu University, Zhenjiang 212013, China

Abstract: To improve the wear resistance of brake disks, the Ni60A coating was prepared on 20CrNiMo steel using laser cladding by optical fiber-based laser system. The microstructure, composition uniformity, hardness, dry-sliding wear performance, and friction and wear mechanism of the Ni-based alloy coating were investigated. The results show that the coating consists of γ-Ni, $M_{23}C_6$, Ni-Cr-Fe, Ni_3B, [Fe, Ni], $FeNi_3$, NiC, FeNi, and other phases. The average microhardness $HV_{0.3}$ of Ni-based alloy coating is 4600 MPa, which is 2.63 times higher than that of the 20CrNiMo steel substrate. Compared with the substrate, the coating exhibits lower average friction coefficients under working condition of high load and high temperature, and the wear resistance significantly improves. When the load is 150 N, the wear resistance of the coating increases by 15.3 and 22.0 times at room temperature and 400 °C, respectively. With the increase of temperature and load, the wear mechanism of the coating changes from abrasive and adhesive wear to oxidative and abrasive wear.

Key words: brake disc; laser cladding; 20CrNiMo steel; microstructure; high temperature friction and wear

Brake disks are the most important load-bearing components of a brake system. To ensure the safety of rail trains, the major daily task of the maintenance staff is to check and repair cracks on the disk surface resulting from friction and wear. The methods for repairing cracks are mainly sanding and polishing, which reduce the thickness of brake disks. A brake disk must be scrapped when the thickness reduction is above 2 mm. The assembly and disassembly processes are complicated, and the axle is prone to damage during these processes. The maintenance costs of brake disks are very high[1-3]. Because cracks usually appear on the disk surfaces, laser cladding, as an additive manufacturing technique, has become a hot research topic recently.

In order to improve the friction and wear properties of the brake disc strengthened by laser cladding, the primary task is to improve the quality of the coating and its adhesion with the substrate. Li et al[4] carried out the nonlinear fitting between the process parameters and the morphology of the single channel coating by neural network, which reduces the defects such as cracks and pores in the coating, and improves the wear resistance of the coating[4,5]. Narayanan et al[6] revealed that the rise in circumstance temperature contributes to the reduction of cracking susceptibility in the laser cladding coating. The suitable circumstance temperature is ~600 °C, at which a relatively high wear resistance can be maintained on the premise that the residual stress is effectively released. It is observed that laser cladding causes a triaxial compressive residual stress field in the coating and near the interface, and a tensile stress field in the parent material. Wear effect on residual stress redistribution is located at the surface of the specimen[7]. Luo et al[8] studied the effect of Mo and Ni on the columnar crystal in the interface layer between the coating and substrate, and revealed the influence of columnar crystal on the properties of the coating. In addition, controlling the solidification rate of materials in the laser cladding process improves the quality of coating, and the related methods are shown as follows: preheating the workpiece[9] and forced-cooling the workpiece by liquid nitrogen[10], laser remelting of

Received date: July 22, 2020
Foundation item: National Natural Science Foundation of China (51801076); Natural Science Research of Jiangsu Higher Education Institutions of China (18KJB430009); Jiangsu Province Postdoctoral Science Foundation (1601055C); Senior Talents Research Startup of Jiangsu University (14JDG126)
Corresponding author: Liu Guanglei, Ph. D., Associate Professor, School of Materials Science and Engineering, Jiangsu University, Zhenjiang 212013, P. R. China, E-mail: liugl@ujs.edu.cn

the coating[11], and applying external energy fields[12] (magnetization, ultrasonication, and specific energy fields) with laser cladding to stir the molten pool. For cladding materials, researches show that the rare-earth elements can refine the grains and reduce the porosity, cracks, and other defects in a laser-clad Ni60A coating, which significantly decreases the coefficient of friction of the coating and improves the wear resistance of the substrate[13,14]. It is found that a laser-clad composite coating made from a mixture of Ni60A powder and ceramic particles (such as WC and B_4C) can also improve the wear resistance of the substrate[15-17].

In summary, Ni-based alloys as a cladding material have been broadly employed in the surface strengthening of metallic components. However, there are few studies on the wear resistance of the coating at high temperature and the use of laser cladding for brake disk reparation. Therefore, this research reported the effect of Ni60A alloy coating fabricated by laser cladding on the strengthening of 20CrNiMo steel, which is a common material for brake disks of high-speed rail trains. The dry-sliding wear performance of the substrate was compared with that of the coating under various loads and temperatures, laying the theory and application foundations for repairing brake disks to extend service life.

1 Experiment

The substrate for laser cladding was commercial 20CrNiMo steel and it was cut into cylindrical plate with a diameter of 100 mm and a length of 15 mm. The composition is shown in Table 1. The cladding powder was Ni60A alloy with a particle size of 45~90 μm. The composition and particle morphology are shown in Table 2 and Fig.1, respectively.

Laser cladding was performed by a disk-type optical fiber laser generator (TruDisk 6002) with a rated power of 6 kW, fiber diameter of 0.2 mm, and wavelength of 1064 nm. A powder feeder (GTV) was used to deliver the powder with Ar gas (99.9% purity) at a flow rate of 10 L/min during the cladding process. A 6-axis robot (KUKA) with a movement precision of 0.05 mm was used. Four-way uniaxial powder feeding was achieved by integrating a laser cladding nozzle, an optical fiber laser generator, a protective gas tube, and a powder feeder. According to the previous experimental results, laser-clad multitrack coatings were deposited with the laser power of 2000 W, scan rate of 350 mm/min, spot size of 3 mm, overlap ratio of 30%, and powder feeding rate of 9.4 g/min.

Wear tests of the as-prepared specimens were performed on a microchip-controlled high-temperature friction and wear testing machine (MMU-5GA) with an attached sensor to

Table 1 Composition of 20CrNiMo steel (wt%)

C	Si	Mn	Cr	Ni	Mo	Fe
0.17~0.23	0.15~0.3	0.7~0.9	0.4~0.6	0.4~0.7	0.15~0.25	Bal.

Table 2 Composition of Ni60A powder (wt%)

C	B	Si	Cr	Fe	Ni
0.5~1.0	3~4.5	3.5~5.5	15~20	≤5.0	Bal.

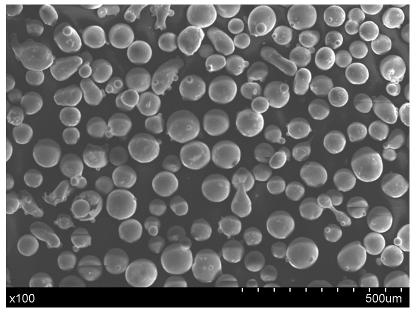

Fig.1 Morphology of Ni60A alloy powder

determine the coefficient of friction. After laser cladding, specimens with a diameter of 4.6 mm and a thickness of 12.7 mm were obtained via wire cutting. The friction pair for wear testing was a GCr15 steel disc with the diameter of 54 mm and thickness of 8 mm. Before testing, the surfaces of the specimens and friction pair were sanded and polished with 400#~1000# sandpaper, washed in an ultrasonic cleaner, and then air-dried. The mass of the specimens before and after the wear test was measured using an electronic scale with the precision of 0.1 mg. The wear test was performed under the dry-sliding condition at temperatures of 25, 200, and 400 °C with the loads of 100 and 150 N, rotation speed of 50 r/min, and duration of 20 min.

The average friction coefficient can be calculated by Eq.(1) as follows:

$$\mu=M/(RF) \tag{1}$$

where μ is the friction coefficient, M is the friction torque, R is the radius of the specimen sliding on the friction pair, and F is the applied load.

The wear mass loss can be calculated by Eq.(2) as follows:

$$\Delta M=m_1-m_2 \tag{2}$$

where ΔM is the mass loss after the wear test; m_1 and m_2 are the specimen mass before and after wear test, respectively.

The microstructures of the clad layers before and after the wear test were characterized using a field-emission scanning electron microscope (FESEM, FEI Nova Nano 450). The elemental composition at various locations of the specimens with different processing parameters was analyzed using an energy-dispersive X-ray spectroscope (EDS). Phase analysis of the clad layer was performed using an X-ray diffraction instrument (XRD, D/MAX2500PC). The microhardness of the specimens was acquired using a hardness tester (FM-ARS900).

2 Results and Discussion

2.1 Microstructure and microhardness

Table 3 and Fig. 2 show the mechanical properties and microstructure of the 20CrNiMo steel substrate, respectively. The microstructure mainly consists of ferrite and pearlite.

Fig.3 and 4 show the microstructures and XRD patterns of the Ni60A alloy clad layer, respectively. The 20CrNiMo steel mainly consists of Fe, Ni-Cr-Fe, and Fe-Cr phases. The clad

Table 3 Mechanical properties of 20CrNiMo steel

Yield strength/MPa	Tensile strength/MPa	Elongation/%	Hardness, $HV_{0.3}$/MPa
961	1231	10.5	1750

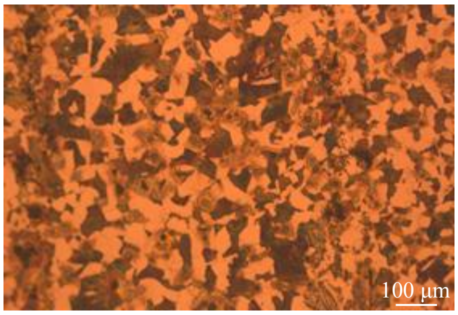

Fig.2 Microstructure of 20CrNiMo steel substrate

layer consists of γ-Ni, $M_{23}C_6$, Ni-Cr-Fe, Ni_3B, [Fe, Ni], $FeNi_3$, NiC, and FeNi phases. The EDS results indicate that the interface between the substrate and the clad layer is mainly the solid solution γ-(Ni, Fe), as shown in the Fig.3a, because both Ni and γ-Fe have face centered cubic (fcc) crystal lattice. Ni atoms in the molten pool tend to nucleate on the surface of γ-Fe, forming a solid solution phase and gradually becoming a Ni-rich solid solution of γ-(Ni, Fe), which indicates a good metallurgical bonding between the substrate and the clad layer. Also, the newly formed γ-(Ni, Fe) in the region near the interface contains a large amount of carbides, and the multi-component eutectics formed by reactions between C and Cr, Fe, and Ni are uniformly distributed at the grain boundaries. In the middle region of the clad layer, as shown in Fig.3b, a strong directionality of the temperature gradient and a large number of dendrites emerge. The eutectic structures solidified from the residual liquid between the dendrites mainly consist of $M_{23}C_6$ (M=Fe, Ni, Cr) and Cr_3Ni_2Si. In the surface region of the clad layer, as shown in Fig.3c, the number of equiaxed grains increases which appear along with the dendrites and eutectics.

Fig. 5 shows the elemental distributions at the interface of Ni60A alloy clad layer, and an increasing concentration of Fe atoms from the coating towards the substrate can be observed. The clad layer contains a large number of Ni, Cr, and Si, whereas the concentrations of these atoms decrease at the interface and disappear in the substrate. Therefore, both the clad layer and the transition interface have no defect, such as cracks and pores, possessing a lower dilution rate. These observations suggest that the processing parameters of laser cladding are proper.

Fig. 6 presents the microhardness distribution in the clad layer and substrate. The average hardness $HV_{0.3}$ of the substrate is 1750 MPa, and that of the coating is 4600 MPa with the highest value of 4780 MPa. Thus, the Ni60A alloy

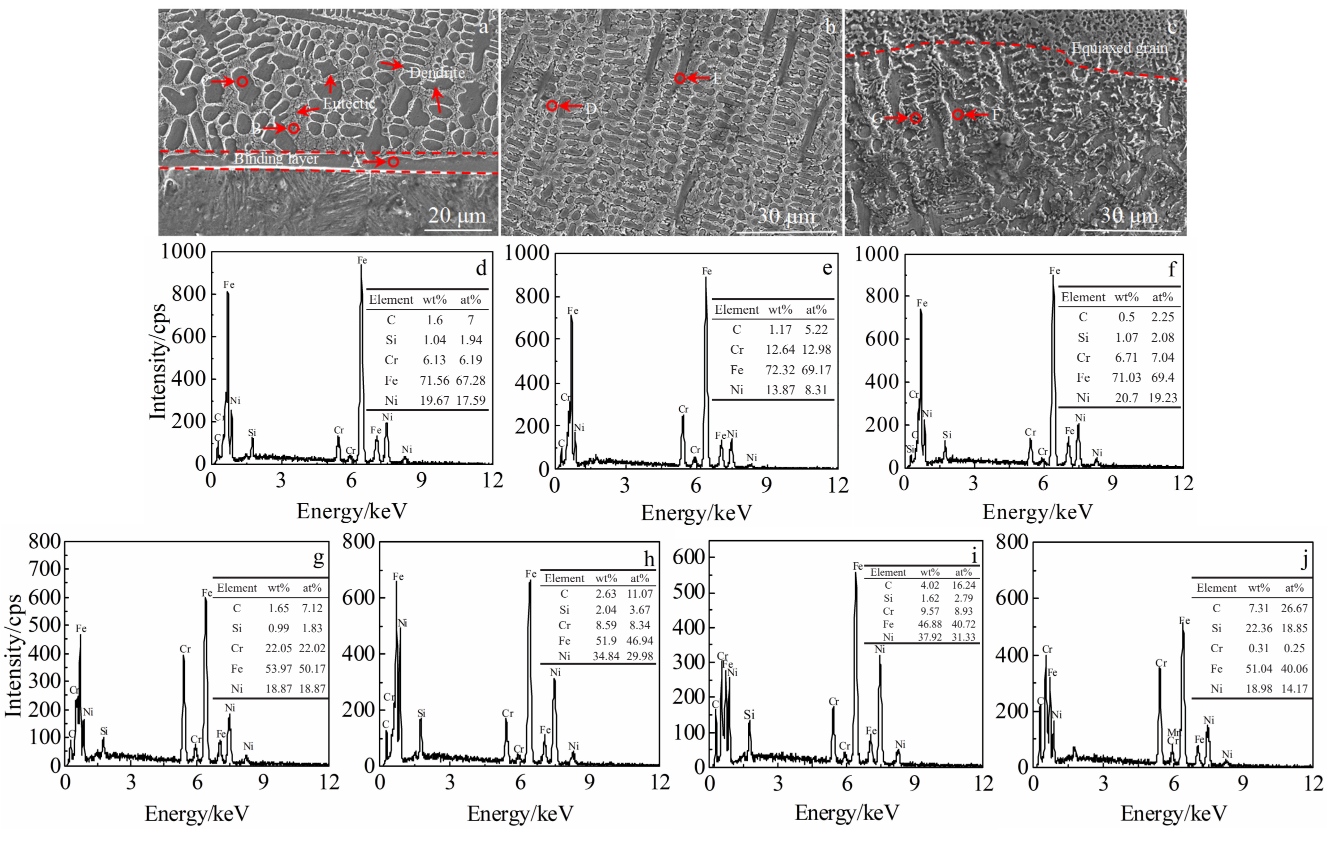

Fig.3 Morphologies of interface (a), middle zone (b), and top surface (c) of Ni60A alloy coating; EDS spectra of point A (d), B (e), C (f) in Fig.3a, point D (g), E (h) in Fig.3b, point F (i) and G (j) in Fig.3c

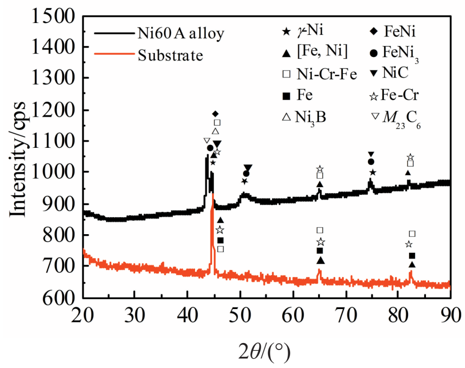

Fig.4 XRD patterns of Ni60A alloy coating and substrate

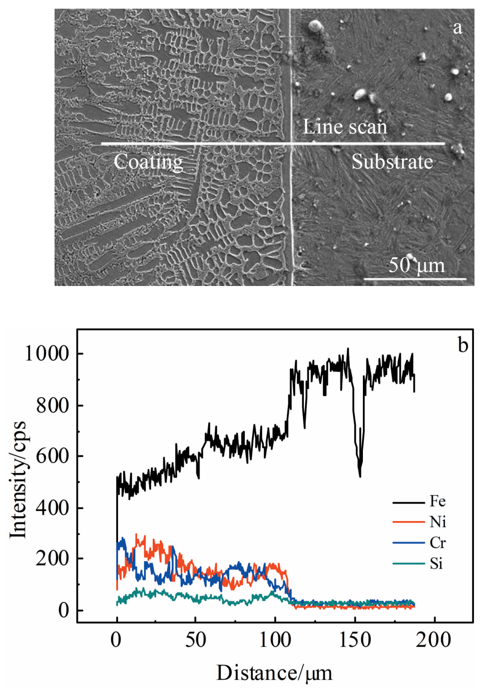

Fig.5 Microstructure (a) and element distribution (b) of specimen with Ni60A alloy coating

clad layer actually provides abundant carbides, and the multi-component eutectics distributed uniformly in the γ-(Ni, Fe) solid solution substrate significantly improve the surface hardness.

2.2 Friction and wear properties

Fig. 7 shows the wear mass loss of coated and uncoated specimens. The 20CrNiMo steel substrate (uncoated specimen) shows a favorable wear resistance at 400 °C, but an evident wear mass loss at room temperature. The wear resistance is notably enhanced due to the existence of Ni60A alloy coating. When the load is 150 N, the wear mass loss at room temperature of uncoated specimen is 29 mg, whereas that of the coated specimen is 1.9 mg, decreasing by nearly 15.3 times. Under the condition of temperature of 400 °C and load of 150 N, the wear mass loss of the uncoated specimen is 2.2 mg, whereas that of coated specimen is 0.1 mg, decreasing by 22.0 times. The 20CrNiMo steel has excellent wear resistance

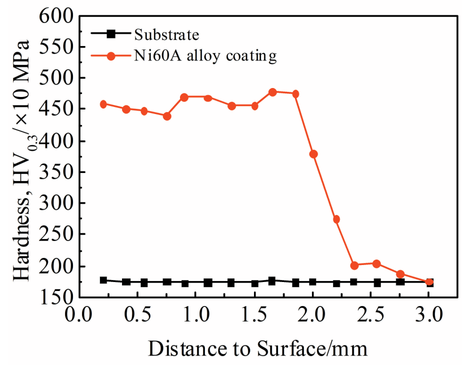

Fig.6 Microhardness $HV_{0.3}$ distribution of Ni60A alloy coating and substrate

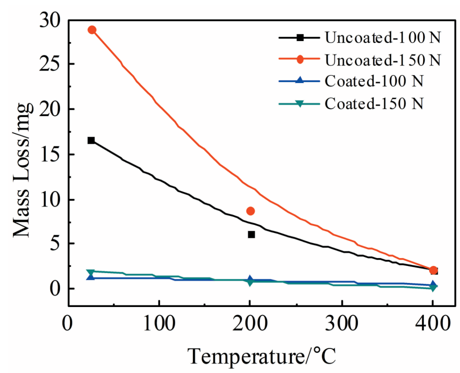

Fig.7 Wear mass loss of coated and uncoated specimens under different loads

properties at high temperature, and Ni60A coating can further improve the related properties[18,19].

The 20CrNiMo steel has good heat resistance and exhibits better wear resistance at high temperatures than it does at room temperature. The average friction coefficient of the coated and uncoated specimens is shown in Fig. 8, which becomes smaller at higher temperatures because the elevated temperature and applied load lead to the softening of micro-bumps on the surface and plastic deformation, respectively. The average friction coefficient of the coated specimen changes slower with the temperature or load, indicating a better heat and oxidation resistance. Thus, the coated specimen exhibits a better and more stable wear performance.

2.3 Friction and wear behavior

Fig.9 and Table 4 show the wear morphologies of uncoated specimen and related EDS point analyses, respectively. Under the condition of temperature of 25 °C and load of 100 N, the specimen shows obvious peeling and adhesive wear (Fig.9a). With increasing the temperature during the wear test, the abrasion debris is oxidized and adhered to the substrate, causing a higher oxygen concentration in the adhesive region (P1). The low oxygen concentration in the non-adhesive region (P2) suggests that this region is less affected by oxidation. At this point, the wear mechanism is mainly peeling

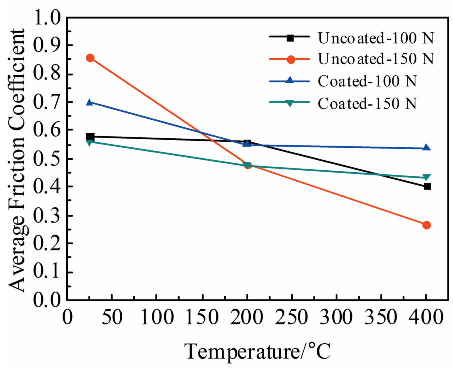

Fig.8 Average friction coefficient of coated and uncoated specimens under different loads

and adhesive wear. Under the condition of temperature of 25 °C and load of 150 N (Fig.9b), the aggressive wear and plastic deformation can be observed on the surface, and the region of adhesive wear expands with aggravated oxidation (P3), indicating that the wear mechanism changes to severe adhesive wear and slight oxidative wear. Under the condition of temperature of 200 °C and load of 100 N, (Fig.9c), the ditches and peeling and adhesive wear can be observed on the surface. When the load increases to 150 N (Fig.9d), more deep ditches emerge. Element contents of P4 and P5 suggest that the oxygen concentration and the oxidized area in the peeling and adhesive regions increase with increasing the temperature, and the wear mechanism is a combination of adhesive wear and abrasive wear. Under the condition of temperature of 400 °C (Fig.9e and 9f), shallower and wider ditches can be observed, and the surface exhibits slight adhesive wear. Analyses of P6,

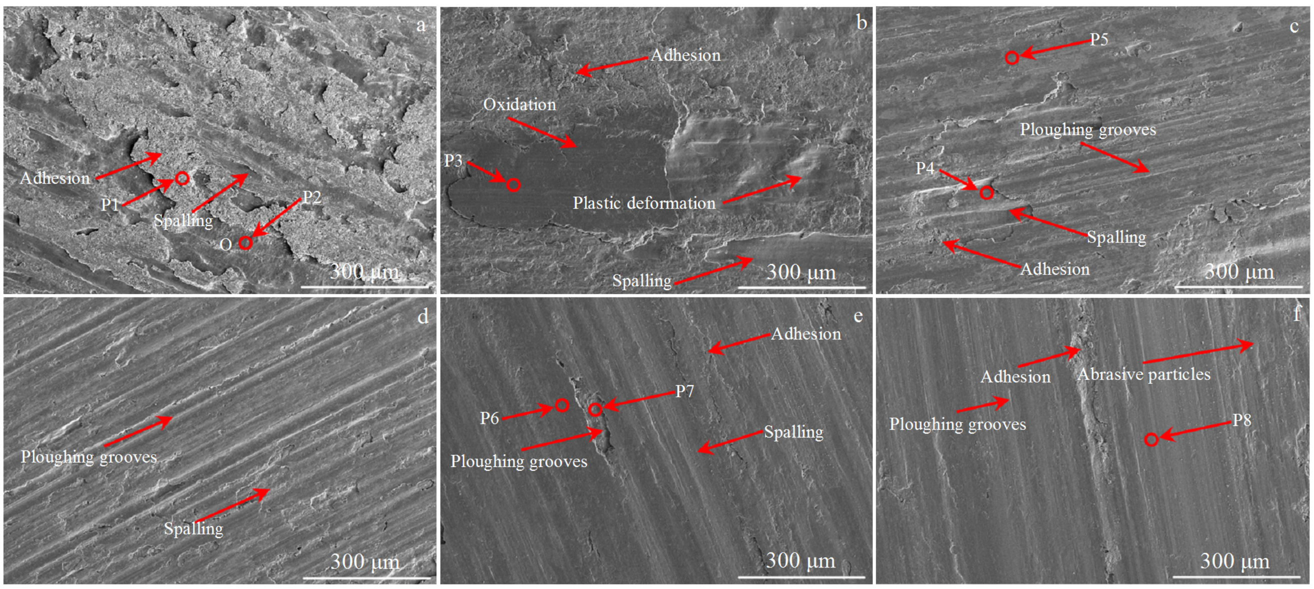

Fig.9 Worn surface morphologies of uncoated specimen under different conditions: (a) 100 N, 25 °C; (b) 150 N, 25 °C; (c) 100 N, 200 °C; (d) 150 N, 200 °C; (e) 100 N, 400 °C; (f) 150 N, 400 °C

P7, and P8 indicate that oxidation becomes more aggravated, and the wear mechanism is oxidative and abrasive wear.

Fig.10 presents the wear morphologies of the coated specimen. Under the condition of temperature of 25 °C and load of 100 N (Fig.10a), the ditches are obvious on the wear surface, suggesting that the wear mechanism is abrasive wear. P1 shows no oxygen in the wear surface, and the Ni60A alloy clad layer has better oxidation resistance. Under the condition of temperature of 25 °C and load of 150 N (Fig.10b), the ditches and slight plastic deformation can be observed. Analyses of P2 and P3 suggest that the abrasion debris is more vulnerable to oxidation than the substrate, which causes a higher oxygen concentration in the adhesive region. The wear mechanism is mainly abrasive and slight adhesive wear. Under the condition of temperature of 200 °C (Fig.10c and 10d), the number of ditches on the wear surface increases with the load, and the wear mechanism changes to abrasive wear. Considering the analyses of P4, P5, and P6, the Ni60A alloy clad layer is more prone to oxidation after peeling or damage, which adversely affects the wear resistance. When the temperature is 400 °C (Fig.10e and 10f), the surface of Ni60A alloy clad layer softens and undergoes plastic deformation under the combined effect of temperature and pressure. The ditches become fuzzy, and the surface is smoother, suggesting that the coefficient of friction is lower. The wear mechanism is oxidative and abrasive wear, resulting in a better wear performance.

In summary, peeling and adhesive wear significantly affects the wear resistance of 20CrNiMo steel, while abrasive and oxidative wear shows a relatively mild effect. With the existence of Ni60A alloy coating via laser cladding to repair

Table 4 EDS analyses results of points P1~P8 in Fig.9 (wt%)

Point	C	O	Fe	Mn	Cr
P1	0.39	12	86.78	0.82	-
P2	0.37	2.77	95.67	1.19	-
P3	0.25	17.65	82.10	-	-
P4	0.14	6.12	93.74	-	-
P5	0.53	15.25	84.22	-	-
P6	-	23	75.61	-	1.39
P7	-	8.17	89.95	-	1.99
P8	0.22	23.26	76.53	-	-

the surface of the steel (especially at elevated temperatures), oxides or oxidized scales form on the surface. As the hard phases, such as carbides and multiphase eutectics, disperse in the clad layer, the microstructure of wear surface changes to a composite structure consisting of a soft γ-(Ni, Fe) solid solution and uniformly distributed hardening phases. This composite structure is beneficial to the wear resistance[20]. Also, the softening of the surface at high temperatures leads to the plastic deformation under different loads, resulting in a smoother surface and a lower coefficient of friction, thereby improving the wear resistance.

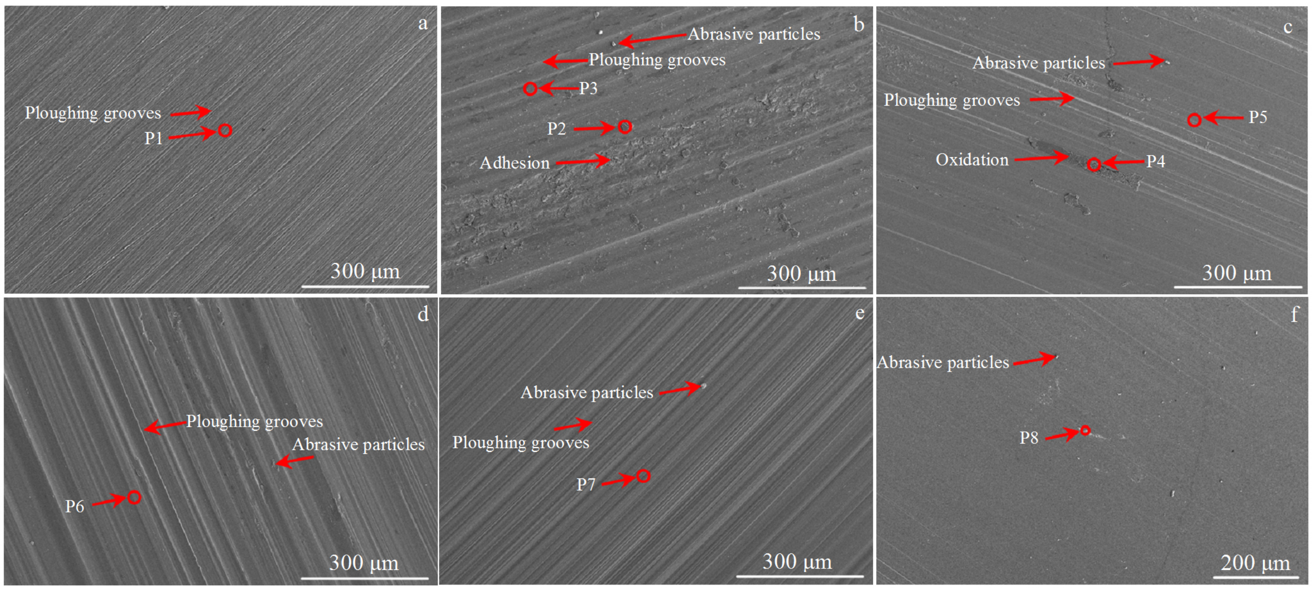

Fig.10 Worn surface morphologies of coated specimen under different conditions: (a) 100 N, 25 °C; (b) 150 N, 25 °C; (c) 100 N, 200 °C; (d) 150 N, 200 °C; (e) 100 N, 400 °C; (f) 150 N, 400 °C

Table 5 EDS analyses results of points P1~P8 in Fig.10 (wt%)

Point	C	O	Si	Cr	Fe	Ni
P1	-	-	2.52	17.22	28.29	51.35
P2	1.11	10.37	2.63	15.07	31.61	39.20
P3	-	1.33	2.17	22.83	26.95	46.72
P4	-	16.87	0.83	7.93	60.03	14.35
P5	0.8	-	1.73	27.35	32.53	37.59
P6	2.27	5.93	3.03	10.42	40.17	38.18
P7	0.7	-	2.48	17.74	29.90	48.18
P8	-	12.08	1.81	11.07	31.51	38.20

3 Conclusions

1) The Ni60A alloy clad layer mainly consists of γ-(Ni, Fe) solid solution, abundant carbides which are uniformly distributed, and multiphase eutectics. The coated specimen has a higher hardness $HV_{0.3}$ of 4600 MPa than the substrate (1750 MPa), indicating a significant increase in the hardness due to the Ni60A alloy clad layer.

2) The coated specimen exhibits notably less wear mass loss and a lower average coefficient of friction than the substrate.

3) With increasing the temperatures and loads, the wear mechanism of 20CrNiMo steel changes from peeling and adhesive wear to abrasive wear, whereas for the coated specimen, the wear mechanism changes from abrasive and adhesive wear to abrasive and oxidative wear.

4) At high temperatures, the Ni60A alloy clad layer exhibits a favorable wear performance because of the oxidation of the wear surface. Thus, the oxides or oxidized scales form, improving the surface hardness. The soft phase on the wear surface causes plastic deformation, resulting in a smooth surface and a low coefficient of friction.

References

1 Shi L B, Wang F, Ma L *et al. Tribology International*[J], 2018, 127: 533

2 He C G, Chen Y Z, Huang Y B *et al. Engineering Failure Analysis*[J], 2017, 79: 889
3 Wu Ying, Liu Yan, Chen Hui *et al. Surface and Coating Technology*[J], 2019, 358: 98
4 Li Hongyu. *Thesis for Master*[D]. Chengdu: Southwest Jiaotong University, 2019 (in Chinese)
5 Jing X, Luo K Y, Sun G F *et al. Lasers in Engineering*[J], 2017, 36(4-6): 319
6 Narayanan A, Mostafavi M, Pirling T *et al*. *Tribology International*[J], 2019, 140: 105 844
7 Tao Yangfeng, Li Jun, Lv Yinghao *et al*. *Optics and Laser Technology*[J], 2017, 97: 379
8 Luo K Y, Xu X, Zhao Z *et al. Journal of Materials Processing Technology*[J], 2019, 263: 50
9 Li Qingtang, Lei Yongping, Fu Hanguang *et al. Rare Metals*[J], 2018, 37(10): 852
10 Zhou Jianzhong, Wang Songtao, Xu Jiale *et al. Rare Metal Materials and Engineering*[J], 2019, 48(2): 500 (in Chinese)
11 Zhou Shengfeng, Xu Yongbo, Liao Bangquan *et al. Optics and Laser Technology*[J], 2018, 103: 8
12 Zhang Nan, Liu Weiwei, Deng Dewei *et al. Optics and Laser Technology*[J], 2018, 108: 247
13 Zhao Ning, Tao Li, Guo Hui *et al. Rare Metal Materials and Engineering*[J], 2017, 46(8): 2092
14 Zhang Hongxia, Yu Huijun, Chen Chuanzhong. *Science and Engineering of Composite Materials*[J], 2017, 24(4): 541
15 Yang Lin, Yu Tianbiao, Li Ming *et al. Ceramics International*[J], 2018, 44(18): 22 538
16 He Xinghua, Xu Xiaojing, Ge Xiaolan *et al. Rare Metal Materials and Engineering*[J], 2017, 46(4): 1074
17 Huang Can, Tang Yizhou, Zhang Yongzhong *et al. Rare Metals*[J], 2017, 36(7): 562
18 Zhong Lin, Wei Gang, Wang Guorong *et al. Proceedings of the Institution of Mechanical Engineers Part J: Journal of Engineering Tribology*[J], 2019, 233(9): 1293
19 Hu Jinkang, Liu Ying, Zhao Xueyang *et al. Applied Physics A: Materials Science & Processing*[J], 2019, 125(6): 390
20 Liu Guanglei, Li Yushan, Li Chao *et al. Rare Metal Materials and Engineering*[J], 2019, 48(2): 620

激光熔覆 Ni60A 涂层对 20CrNiMo 合金高温干滑动摩擦磨损性能的影响

刘光磊，曹宇豪，冀思博，余　辉，蒋文能，李茂军，司乃潮
(江苏大学 材料科学与工程学院，江苏 镇江 212013)

摘　要：为改善制动盘材料的耐磨性能，选用Ni60A粉末，利用光纤激光器对20CrNiMo铸钢进行激光熔覆处理，研究了涂层的微观组织、成分均匀性、硬度、干滑动磨损性能及其损伤机制。结果表明：涂层主要由γ-Ni、$M_{23}C_6$、Ni-Cr-Fe、Ni_3B、[Fe, Ni]、$FeNi_3$、NiC、FeNi等相构成，涂层平均显微硬度$HV_{0.3}$为4600 MPa，较基体提高2.63倍。与基体相比，涂层在高载、高温工况下具有更小的平均摩擦系数，耐磨性得到显著提升。当载荷为150 N时，在室温和400 ℃时，耐磨性分别提高15.3和22.0倍。随温度和载荷的增加，涂层的损伤机制由磨粒和粘着磨损向氧化和磨粒磨损转变。

关键词：制动盘；激光熔覆；20CrNiMo 合金钢；微观组织；高温摩擦磨损

作者简介：刘光磊，男，1983年生，博士，副教授，江苏大学材料科学与工程学院，江苏 镇江 212013，E-mail：liugl@ujsedu.cn